An ECG Delineation and Arrhythmia Classification System using Slope Variation Measurement by Ternary Second-Order Delta Modulators for Wearable ECG Sensors

Xiaochen Tang, *Member, IEEE* and Wei Tang, *Member, IEEE*

***Abstract*—This paper presents a system for electrocardiogram (ECG) delineation and arrhythmia classification. The proposed system consists of a front-end integrated circuit, a delineation algorithm implemented on an FPGA board, and an arrhythmia classification algorithm. The front-end circuit applies a ternary second-order Delta modulator to measure the slope variation of the input analog ECG signal. The circuit converts the analog inputs into a pulse density modulated bitstream, whose pulse density is proportional to the slope variation of the input analog signal regardless of the instantaneous amplitude. The front-end chip can detect the minimum slope variation of 3.2 mV/ms^2 within a 3 ms timing error. The front-end integrated circuit was fabricated with a 180 nm CMOS process occupying a 0.25mm^2 area with a 151 nW power consumption at the sampling rate of 1 kS/s. Based on the slope variation obtained from the front-end circuit, a delineation algorithm is designed to detect fiducial points in the ECG waveform. The delineation algorithm was tested on a Spartan-6 FPGA. The delineation system can detect the intervals, slopes, and morphology of the QRS/PT waves and form a feature set that contains 22 features. Based on these features, a rotate linear kernel support vector machine (SVM) is applied for patient-specific arrhythmia classification of the ventricular ectopic beat (VEB), supraventricular ectopic beat (SVEB), and heartbeats originating in sinus node. The performance of the proposed system is comparable to the recently published methods while providing a promising solution for the low-complexity implementation of future wearable ECG monitoring systems.**

***Index Terms*—ECG delineation, second-order Delta modulator, ternary circuits, slope variation, fiducial points, patient-specific, machine learning, support vector machine.**

I. Introduction

Cardiovascular disease (CVD) has been recognized as the leading health problem for humans according to the world health organization's estimation [1]. To alleviate such a challenge, many resources have been spent on CVD research [2] to prevent the death caused by CVD [3]. The risk of CVD can be reduced by timely diagnosis, which is highly dependent on the electrocardiogram (ECG) technology. The most important function of ECG is to detect and classify different types of arrhythmia, which reflects the health status of the heart. Some acute arrhythmic symptoms may cause a high death rate if the patient does not receive timely treatment, while some chronic arrhythmia symptoms need to be monitored continuously to prevent further health deterioration. Thus, continuous monitoring of the ECG signal and the timely detection of arrhythmic symptoms from the ECG signal is critical for CVD control. However, most of the current ECG processing still depends on people, especially nurses who have been trained with basic skills to identify basic types of arrhythmia, since the number of cardiologists is limited for the increasing number of patients.

Wearable ECG sensing devices are promising solutions to provide continuous monitoring and arrhythmia classification [4]–[12] with help from telemedicine. However, the current wearable solutions of arrhythmia classification from both academia and industry are still far away from meeting the same level of skills of a nurse. For example, [13] can detect 12 types of arrhythmia but a nurse needs to know about 30 types of arrhythmia to pass the national certification test. In the current industrial solutions, Medtronic Reveal LINQ Insertable Cardiac Monitor (ICM) also relies on telemedicine, which can provide results but with a considerable amount of delay. Other solutions, such as Kardia band and Apple Watch 4, both can only detect one type of arrhythmia of atrial fibrillation, which only happens 2% in the population under 65 years old. One common problem of the abovementioned system is that the raw data transmission occupies a large portion of the power consumption, which limits the recording time so that most of those solutions can only monitor a 30-second episode of ECG. An on-chip ECG processing algorithm may reduce the communication power of wearable devices. In other words, autonomous ECG sensing and processing systems that could perform continuous monitoring and rudimentary arrhythmia classification are highly expected in the future.

Many algorithms have been proposed to perform arrhythmia classifications [9], [11], [15]–[18]. Some recent arrhythmia classification systems are directly applying deep learning algorithms, which usually do not provide an interpretable process. Interpretable means that the intermediate decision process of the algorithm is understandable by humans. Since interpretable arrhythmia classification is important for making human-machine collaborative medical decisions, in this work we follow the typical classification procedures. A typical arrhythmia classification has several steps, including feature extraction, delineation, and classification. First, important information of the raw ECG waveform is extracted as features, such as baseline, slope, and turning points. Second, delineation is performed based on the features of the ECG to identify the

Manuscript was received on May 21, 2021, revised on August 8, 2021, and accepted on September 13, 2021; This work is sponsored by United States National Science Foundation grant 1652944 and 2015573 .

Xiaochen Tang is with the Department of Computer Engineering, Texas A&M University, USA.

Wei Tang is with the Klipsch School of Electrical and Computer Engineering, New Mexico State University, USA.

Correspondence should be addressed to: Wei Tang 1125 Frenger Mall, Las Cruces, New Mexico 88003 USA. E-mail: wtang@nmsu.edu

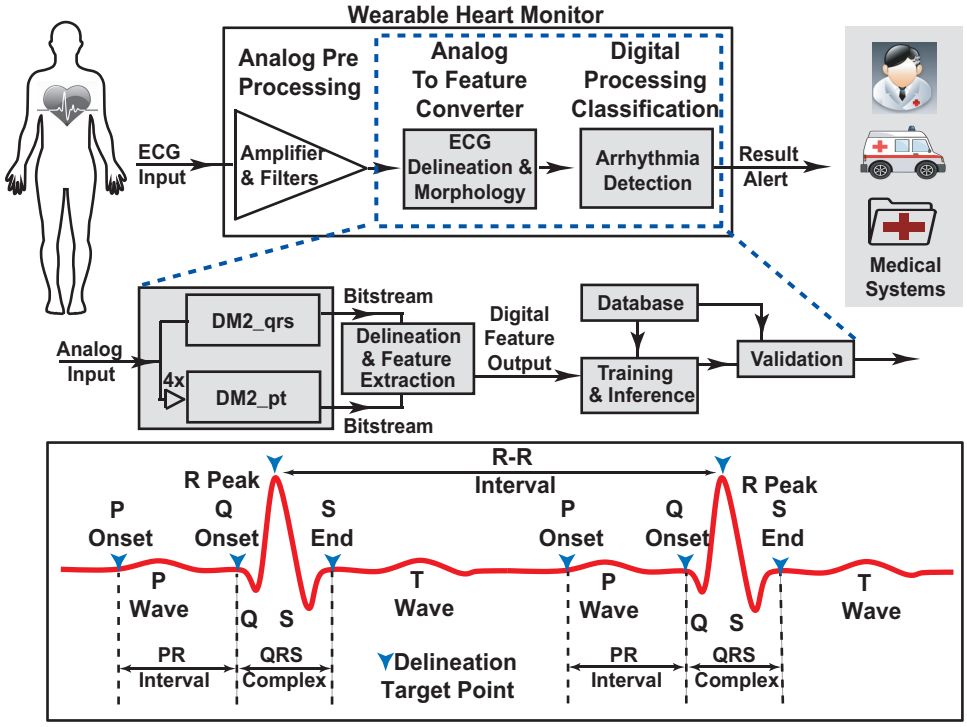

Fig. 1. (Top) Wearable heartbeat monitor system, (Middle) The scope of this work focusing on the parallel ternary second-order Delta Modulator based analog-to-feature converter for delineation and arrhythmia classification, (Bottom) ECG Delineation highlighting the key fiducial points and intervals. Modified from [14].

fiducial points, including the onset, peak, and end-points of the key waves including the P wave for atria depolarization, the QRS complex for ventricular depolarization, and the T wave for ventricular repolarization. Then the final step is arrhythmia classification, which is done by analyzing the wave morphologies and measuring critical timing information. Usually, the wave morphologies include the P wave deflection, QRS complex duration, and ST elevation while the critical timing information of the fiducial points includes the R-R interval, P-R interval, and the duration of the QRS complex. This process is also similar to the procedures of how a nurse is reading the ECG.

One of the biggest challenges in arrhythmia classification comes from P wave detection. Compared to the QRS complex, the P wave usually has a much lower amplitude, which sometimes is even lower than the baseline wandering. Baseline wandering is another critical challenge in ECG signal processing. To overcome these problems, wavelet analysis [19]–[22] becomes the most typical algorithm in conventional ECG processing. Multi-level SVM [23], Frequency Analysis [24], and Adaptive Decision [25] methods were also proposed for ECG processing based on successive-approximation-register (SAR) analog to digital converters (ADCs). However, due to the high computing overhead, wavelet methods are difficult to be implemented on wearable sensors. One reason causing these problems is that a typical ECG sensor is based on the conventional analog-to-digital converter. A regular ADC generates too much data with a high sampling rate, which makes it difficult to extract feature information from a large amount of data. To solve this problem, analog-to-feature converter [26] is proposed, which can directly extract the important features such as slope, peaks, and turning points during the analog-to-digital conversion. Currently, the main methods for such converter include level crossing ADCs, and the Delta modulated analog-to-feature converters [27]. They both convert the input analog waveform into bit-streams and use the pulse density to measure the slope of the waveform. They also offer reduced power by avoiding multi-bit analog-to-digital conversion at each sample.

Nevertheless, these bit-stream based ECG sensors have a common problem of baseline wandering. This makes it difficult to detect a fiducial point in the waveform if such a point is “buried” in the baseline slope and does not become a local peak. For example, in [28] we proposed a Delta modulation based analog-to-digital converter, which converts the analog input into a ternary pulse stream. The converted output pulse stream is a pulse density modulation of the slope of the input analog waveform. While the system is good at measuring the slope, it struggles to measure the peak of the waveform especially the small peaks such as in the P wave. This makes it difficult to perform delineation especially for the low amplitude waves such as the P wave and T wave. Moreover, since baseline wandering may impose additional slopes on the entire waveform, the detection accuracy may drop. A similar situation also applies in the level-crossing based ADCs. Therefore, new analog-to-feature converters are

expected to find the turning points in the input waveforms even in the presence of a large baseline wandering.

To solve the abovementioned challenges, we proposed a new analog-to-digital-converter based on the second-order Delta modulator [14]. The second-order Delta modulator performs a pulse density modulation of the slope variation of the input signal using the oversampling method [29], [30]. The turning point of the input waveform can then be identified. Moreover, the slope variation rate can be measured using a counting window method. Although other second-derivative analog feature extraction circuits [31], [32] were reported before, to the best of our knowledge, this is the first analog-to-feature conversion circuit that can directly measure the slope variation of an analog signal using the Second-order Delta modulator. The second-order Delta modulator circuit is similar to a regular first-order Delta modulator while it uses a first-order Delta modulator as the quantizer. To perform an efficient measurement, a ternary output is applied. The new feature of slope variation is then directly extracted from the output ternary bitstreams. With the help of the slope variation feature, the p-wave delineation can be achieved to help the arrhythmia classification. We also note that the circuit has good handling of baseline wandering since it is only sensitive to slope variation but not sensitive to the slope or the instantaneous amplitude of the analog signal.

This paper is expanded from our previous work [14] of the second-order ternary Delta modulator integrated circuit. In this paper, we extended the scope of [14] by adding the digital feature extraction algorithm and the arrhythmia classification algorithm, the overall system is illustrated in Fig. 1. The main innovation and contribution of this paper include: (1) designed feature extraction methods based on the output bitstreams of the second-order Delta modulator; (2) developed an arrhythmia classifier using a patient-specific rotation-hyperplane support vector machine based on the new features; (3) validated the proposed classification method using the benchmark MIT-BIH database with AAMI standard [33] and compared the results with the first-order Delta-modulator-based feature extractor and classifier from [28]. The novelty of the work focuses on the implementation of a Second-Order Delta Modulator integrated circuit and the proposed algorithm. The proposed system detects the turning points and measures the slope variation rate of the analog waveform. To the best of our knowledge, this is the first reported Second-Order Delta Modulator circuit on ECG signal processing. New concepts have also been proposed such as the slope variation rate of the turning point. The proposed circuit has the advantages of performing delineation and classification with baseline wandering resistance, which is promising for future wearable ECG classification devices. The remaining paper is organized as follows: Section II presents the circuits and systems of the second order Delta modulator and the proposed feature extraction algorithm. Section III introduces the classification method using the features extracted from the second-order Delta modulator. Section IV shows the circuit testing results and the classification results. Section V discusses the advantages, limitations, and future work. Section VI concludes this paper.

II. Circuits and Systems Design

The overall system block diagram is shown in Fig. 1. The system consists of the front-end sensing circuit and the back end digital signal processing block. In this work, we focus on analog-and-digital processing so we assumed that the front-end amplifier has obtained the amplified analog ECG waveform. To obtain accurate processing results, we adapt the parallel processing method proposed in our previous work [28] to separate the QRS and PT channels. The QRS channel uses a lower integration gain to focus on QRS detection while filtering out the small waves and noise. The PT channel relies on the QRS channel to locate the QRS complex to avoid saturation. The second-order Delta modulators convert each channel into two digital bitstreams of pulse density modulation. Then the digital processing unit performs feature extraction and classification using the bitstreams from the second-order Delta modulator. The patient-specific classification method using the rotation hyperplane [34] is applied to classify arrhythmic heartbeats over normal heartbeats. The classification result is then recorded and compared to the benchmark database.

A. Ternary second-order Delta modulator circuits

The second-order Delta modulator performs a pulse density modulation of the input analog signal, in which the pulse density is proportional to the input slope variation. Since a ternary output is applied, the circuit is essentially a 1.5 bit analog-to-digital converter which calculates the second derivative of the input signal. The second-order Delta modulator for P/T waves has an extra preamplifier with a gain of 4 so it is more sensitive to a lower slope variation compared to the second-order Delta modulator for QRS detection. The positive or negative output pulses of the ternary comparator are generated only when the slope of the input signal has an up or down variation. Regardless of the initial input slope, an upward-turning point (UTP) of the analog input results in positive output pulses (POSONE) while a downward-turning point (DTP) leads to negative output pulses (NEGONE). The output pulses from both the second-order Delta modulators are processed digitally to extract timing information of the fiducial points and analyze the P wave morphology for arrhythmia classification.

The ternary second-order Delta modulator circuit consists of two integrators, a quantizer, and two subtractors. The simplified schematic is shown in Fig. 2. Two integrators are applied in the feedback loop. Each integrator consists of a sampling capacitor Cs, an integrating capacitor Ci, and an operational trans-conductance amplifier (OTA). The ternary quantizer uses two comparators and compares the second integrator output with two pre-defined thresholds. If the input signal has a constant slope, the output of the second quantizer is then between the two thresholds so no output pulse is triggered. The capacitor Csub is the subtraction capacitor that generates and holds the voltage difference between the input signal and the feedback voltages. The OTA circuit is adopted from [35] which uses the recycling folded cascode architecture to enhance transconductance, gain, and slew rate. The comparator

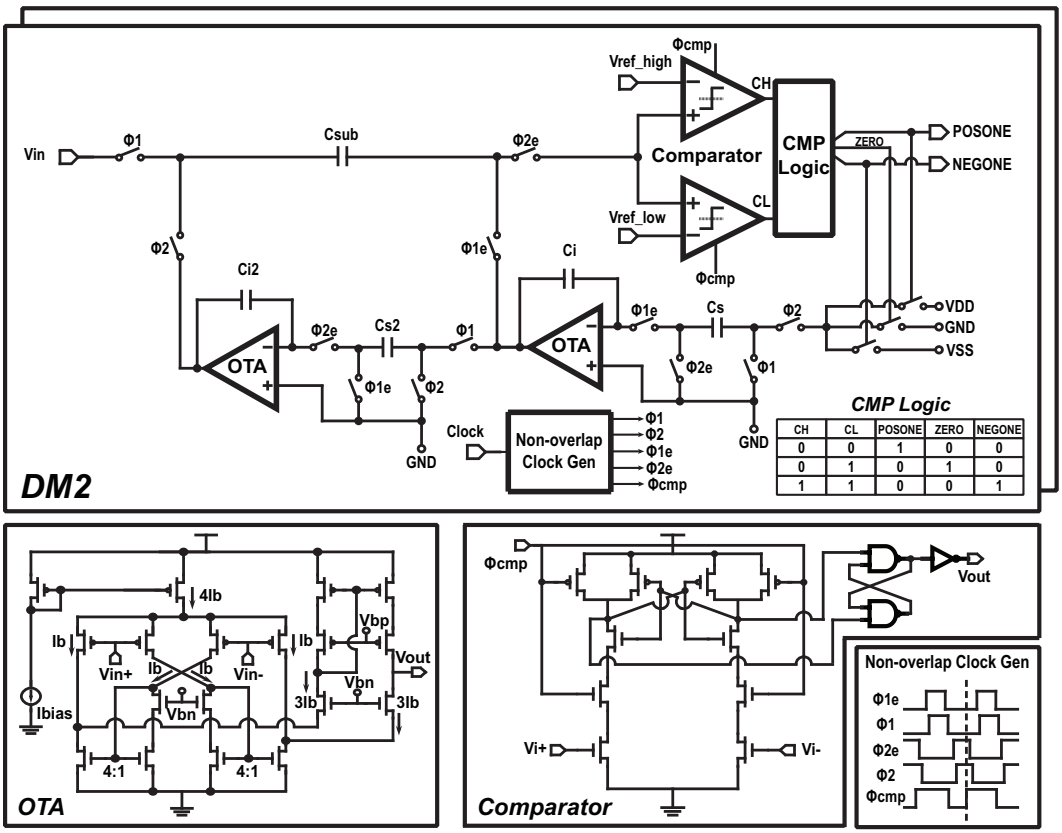

Fig. 2. (Top) Simplified circuit schematic of the ternary second-Order Delta Modulator $DM2$ with the truth table of comparator processing (CMP) logic. (Bottom) Schematic of the OTA (left) and the comparator (right) with the timing diagram of the Non-overlap clock (bottom). Modified from [14].

circuit [36] uses a pseudo-differential topology to avoid static power consumption. The schematics of the OTA and the comparator are shown in Fig. 2. The switching phases of sampling, integration, and comparison are controlled by non-overlapping clocks as also shown in Fig. 2. In the circuit operation, the rising edge of ϕcmp should be earlier than the falling edge of ϕ2e so that the sampling capacitor Cs can be pre-charged with the current ternary state for the coming next integration.

The determination of the gain and threshold voltage is a correlated process, since the amplitude of input signal, integration gain, and reference voltage are mutually affected. The design process has mainly 3 steps. (1) We decide the size of the integration capacitor range due to area limits, then the gain of the second-order delta modulator can be preliminary decided. (2) We set up a $Sinc$ function in MATLAB with assumed QRS complex amplitude and to decide the reference voltage that prevents the second-order delta modulator saturation and make the modulator respond well to the input signal, and also the decided reference voltage should tell enough information since larger reference voltage value means fewer pulses, i.e., less information. (3) We run parameter analysis simulation with several channels of data in the MIT-BIH arrhythmia database, such as record 100 for good signal quality data and record 207 for bad quality data. We then check False-Negative (FN) and False-Positive (FP), and repeat this step with fine-tuning of gain and reference voltage until a satisfying result, then we fix this integration gain and a reference voltage and use it to test all records in the database and design the circuit.

B. Delineation

The output bit-stream from the ternary second-order Delta modulator contains positive or negative pulses. These pulses are generated by the two comparators only when the slope of the input signal has an up or down variation. The output pulses are then processed digitally to perform delineation for locating the fiducial points of the ECG waveform. In the preliminary validation, the digital processing design was implemented on an FPGA, which can be converted into mixed-signal integrated-circuits in future development. The digital processing contains QRS complex detection and P/T wave detection. Each fiducial point and interval are calculated and stored by dedicated digital logic and memory buffers.

The first step of the processing is to locate the QRS complex, which is the most distinct mark in ECG signals. The system locates the QRS complex by counting the number of UTP and DTP in a sliding window. The result is then compared with predefined thresholds to check if the UTP/DTP pulse density meets the standard of the R wave. A positive or negative R wave is detected if a sequence of three consecutive sections of UTP-DTP-UTP or DTP-UTP-DTP meets the pulse density

thresholds in each individual section. After the detection of the R wave, the algorithm searches back to locate the onset point of the Q wave and the peak of the R wave in data caches. The data cache is a first-in-first-out shift register that stores 128 ms bit-streams from the output of the second-order Delta modulator. In the data cache, the search algorithm looks for the first pulse (FiP), which is defined if there is no pulse in its prior 10 clock cycles. Then a pulse cluster (PC) is marked as all the pulses in the next 20 clock cycle window after the FiP. The FiPs before and after the R peak are identified as the onset and the endpoint of the QRS complex.

The P wave and T wave detection are performed with help from the QRS complex detection, which uses similar methods. In particular, the T wave detection starts after a QRS complex is detected while the P wave detection is working in parallel with the R wave detection. This is because in some arrhythmia like the Second or Third degree Atrioventricular Blocks, there may be more than one P wave before each R wave. When the R wave is detected, the P wave detection process is paused and it would resume once a T wave is recognized. The onset, peak, and endpoint of the P wave are obtained from the P/T channel bitstream stored in a data buffer. The P wave morphology is classified using the UTP and DTP information. During these processes, we implemented protection mechanisms to avoid interference from noise or other disturbance. For instance, any single pulse with no neighboring similar pulse within its prior or later pulse cluster window would be considered as a noise pulse in the bit-stream, which is removed. We also applied the duration constraints of each PQRST wave and the intervals between each pulse cluster. These constraints filter out unreasonable pulses in the bitstream. In the last step, the timing information and key intervals are calculated after delineation.

A simplified flowchart of the delineation process is illustrated in Fig. 3. The system starts with the second-order Delta modulator for the QRS detection $DM2\_qrs$ and keeps monitoring the downward slope variation SV_d. The R peak is detected once SV_d reaches a predefined threshold SV_R. Then the algorithm searches backward and forward in the bitstream to find the Q peak and the S peak, respectively. A Q peak candidate is detected when the upward slope variation SV_u is greater than a predefined threshold SV_Q while an S peak candidate is detected when SV_u is greater than another predefined threshold SV_S. Then the algorithm checks if the QRS duration meets the goal of a predefined timing TH_{QRS}, if not the algorithm searches for other Q and S candidates until the fiducial points of the QRS complex can be identified and meet the predefined thresholds of both timing and slope variation. After the delineation of the QRS complex, the algorithm starts checking the bitstream from the second-order Delta modulator for the P and T waves $DM2\_pt$ using the small-wave delineation algorithm (SWD). The algorithm searches the bitstream backward to find the P wave and forward to find the T wave. The SWD searches both SV_d and SV_u in the bitstream to find potential fiducial points of the P waves and T waves using the predefined slope variation of the P/T waves. Once the fiducial point candidates are identified,

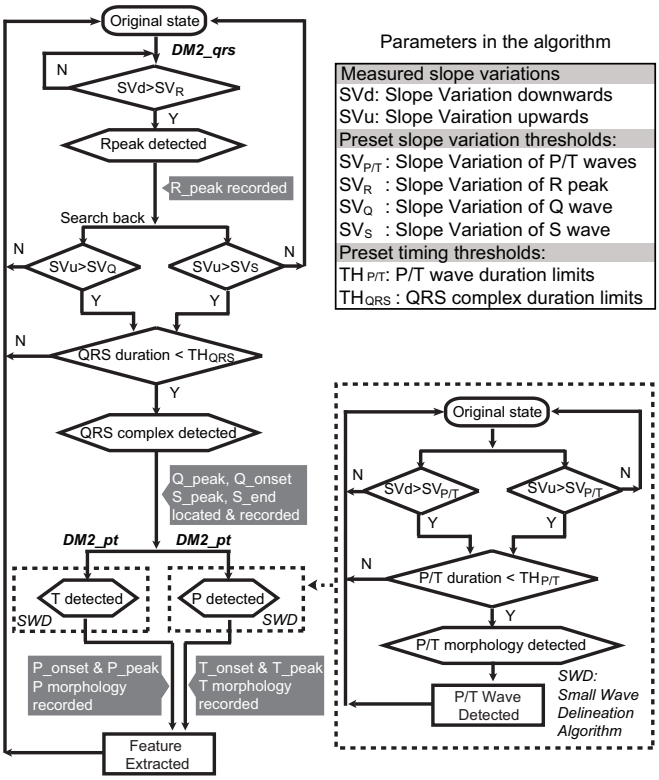

Fig. 3. Delineation algorithm flowchart with measured and preset timing and slope variation parameters.

the algorithm checks the timing of those points to make sure they meet the requirement of the P wave and T wave duration. If the delineation process is successful, the morphology of the P wave and T wave are classified. The morphology of the P waves and T waves include upright, negatively deflected, biphasic +/-, or biphasic -/+. The delineation process concludes with identified fiducial points from the bit-stream and the recorded morphology of the P and T waves.

C. Feature Extraction and Classification

The delineation results directly provide important features for arrhythmia classification. In this work, we calculate 22 features from the delineation results, which include12 intervals, 7 slopes, and 3 morphologies. The 12 intervals are (1) $QRSpk$: the interval from the Q peak to the S peak, (2) $QpkRpk$: the interval from the Q peak to the R peak, (3) $RpkSpk$: the interval from the R peak to the S peak, (4) $PpkRpk$: the interval from the P peak to the R peak, (5) $PonQpk$: the interval from the P onset to the Q peak, (6) $PonQon$: the interval from the P onset to the Q onset, which was also known as the PR interval, (7) $PpkQpk$: the interval from the P peak to the Q peak, (8) $RpkTpk$: the interval from the R peak to the T peak, (9) $QonTpk$: the interval from the Q onset to the T peak, (10) $SpkTon$: the interval from the S peak to the T onset, (11) Prior R-R: the interval between the prior R peak to the current R peak, and (12) Next R-R: the interval between the current R peak to the next R peak. The slope variations include (1) the P wave onset, (2) the P wave peak, (3) the Q wave peak,

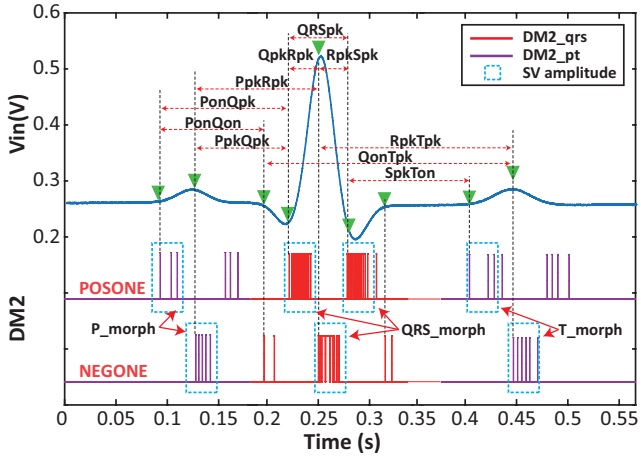

Fig. 4. Key features extracted from the delineation process for arrhythmia classification, including twelve intervals, seven slope variations, and the morphology of three waves.

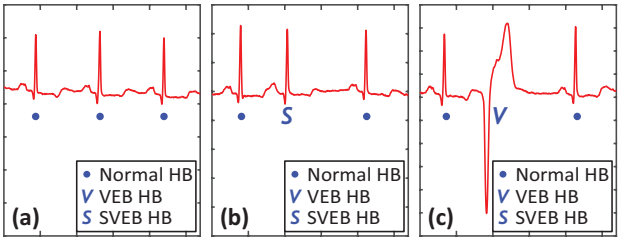

Fig. 5. The goal of the classification is to identify (a) Heartbeats originating in sinus node, (b) SVEB heart beat, and (c) VEB heart beat.

(4) the R wave peak, (5) the S wave peak, (6) the T wave onset, and (7) the T wave peak. The morphology refers to the directions of the waves (upward or deflected), which include (1) P_morph for the P wave morphology, (2) QRS_morph for the QRS complex morphology, and (3) T_morph for the T wave morphology. The features are illustrated in Fig. 4.

The arrhythmia classification is challenging due to the large inter-patient and intra-patient morphology variations of the ECG signal. In this work, we focus on the classification on heartbeats originating in sinus node (class N beat), the supraventricular ectopic beat (SVEB), and the ventricular ectopic beat (VEB). VEB exhibits a bizarre morphology of the QRS complex since the ectopic focuses on ventricles instead of the sinoatrial node. On the other hand, SVEB usually has a normal QRS morphology, in which the QRS complex duration is between 60 and 100 ms. However, the location of the QRS complex in SVEB is abnormal, which results in a variation of the R-R interval. The differences among the normal heartbeat, VEB, and SVEB are illustrated in Fig 5. Other morphologies of the ECG signal make it difficult to form the classifier. For example, the performance of the classifiers is usually evaluated by the MIT-BIH database, in which nearly half of the 48 recordings have multiform Premature Ventricular Contractions (PVC). The PVC morphology makes the classifier modeled by machine learning techniques uneasy to work when the model

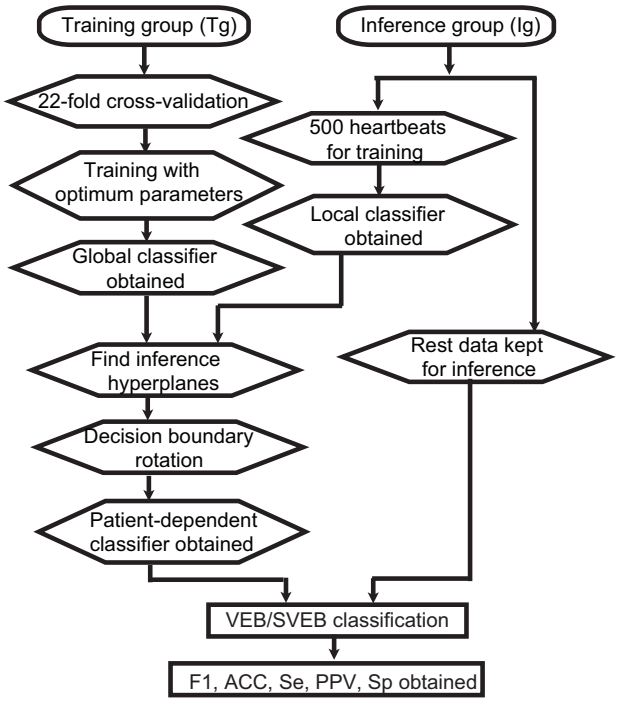

Fig. 6. The flow chart of the classification process.

meets new patients.

A patient-specific classifier becomes a promising method to address the abovementioned problem and improve the classification accuracy. In our prior work, we have proposed a combination of global classification and local classification for patient-specific training [34]. The global classifier is trained by the overall data while the local classifier is trained using some of the data from a specific recording. This combined classifier is validated by cross-validation. Patient-specific classifier brings another advantage of reducing the hardware and power cost when it is implemented on wearable sensors. For instance, although support-vector-machine (SVM) has been widely used to solve practical problems due to its excellent generalization ability, the hardware implementation cost is directly related to its kernel function. It has been shown that a radical basis function (RBF) kernel costs more than 50000 times power consumption per classification compared to a linear kernel [37]. Though linear kernel SVM has a lower classification accuracy, the patient-specific method can partially compensate for the drawback of the linear kernel to improve the accuracy, and balance both the generalization performance and the patient feature's importance enhancement. Therefore, in this paper, we use a linear kernel SVM which rotates the global classifier to a certain angle towards the local classifier to obtain a patient-specific linear SVM classifier.

For patient specific design, the recordings of the MIT-BIH Arrhythmia database are divided into two groups following data split method in [38], the training data group (T_g): 101, 106, 108, 109, 112, 114, 115, 116, 118, 119, 122, 124, 201, 203, 205, 207, 208, 209, 215, 220, 223, 230, and the inference

data group (I_g): 100, 103, 105, 111, 113, 117, 121, 123, 200, 202, 210, 212, 213, 214, 219, 221, 222, 228, 231, 232, 233, 234. The four paced recordings 102, 104, 107, and 217 are not included in T_g and I_g.

A detailed classification process is illustrated in Fig. 6. The process starts from the T_g data. After a 22-fold cross-validation and parameter optimization, the global hyperplane is obtained which is referred to as the global classifier. Then the local classifier is formed by training with 500 heartbeats from each record in I_g. The global classifier and the local classifier are then combined to find the inference hyperplane using the hyperplane rotation method to obtain the patient-specific classifier. After that, the rest data from each record in I_g are used to test the inference accuracy of the VEB/SVEB classification. Finally, the classification performance, including the F1 score, Accuracy, Specificity, Sensitivity, and Precision, are calculated.

One of the main advantages of the proposed feature extraction and classification method is that it achieved an interpretable arrhythmia classification. Medical decisions are essentially made by humans including nurses and cardiologists, who are reading the ECG signal by their intervals and morphology. While humans could make mistakes due to fatigue or lack of practice, automatic classifications could assist people by providing suggestions. However, one of the most important features of the system is to let the human understand how the algorithm makes a certain decision, especially when the machine result is different from the decision made by people. Therefore, an interpretable arrhythmia classification approach is critical to achieving the human-machine collaborative decision making [39]. Most of the current arrhythmia classification systems are based on deep-learning [10], [16], [40]–[42] and wavelet transform [10], [43], in which the intermediate decision process is difficult to be understood by people. Since the proposed method uses the turning points, intervals, and morphology of the ECG signal, it is much easier to be interpretable by people. This makes the proposed system a promising solution for future human-machine collaborative medical decision making.

III. Experimental Results

A. Integrated Circuit Testing Results

The ternary second-order Delta modulator was fabricated with TSMC 0.18um CMOS process. The microphotograph of the fabricated chips with the circuit layout is shown in Fig. 7. The chip occupies 0.248 mm^2. The second-order Delta modulator performs a pulse density modulation of the input slope variation. Example input and output waveforms for UTP and DTP with different slope variation rates are illustrated in Fig. 8. When the input signal has a higher slope variation, the output pulse cluster has a higher pulse density regardless of the initial direction of the slope. Since we focus on ECG delineation and classification, the main task of the second-order Delta modulator is to identify the location of the turning point and measure the slope variation rate. Therefore, the primary performance of the circuit is evaluated by its response time, timing error, sensitivity, and dynamic range.

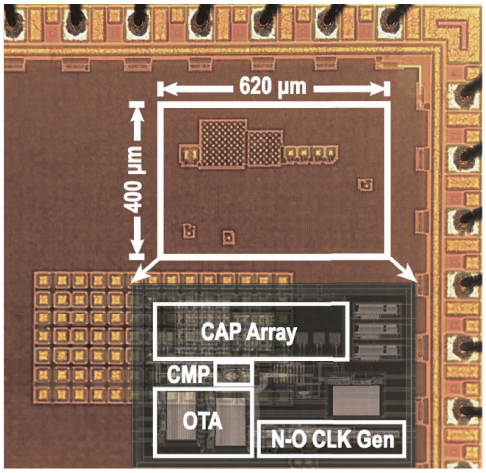

Fig. 7. The microphotograph of the fabricated ternary second-order Delta modulator chip [14].

The response time and timing error are related to identifying the turning point while the sensitivity and dynamic range are related to the capability of measuring the slope variation.

The response time is defined by the timing delay from the turning point of the analog input to the first pulse of the digital output. The timing error measures the standard deviation of the response time. Fig. 9 (Top) presents the delay variation of the turning point detection. The measured mean (m) and standard deviation (s) of the response time are 5.01±2.17 ms for UTP and 5.30±2.40 ms for DTP. The statistics of the delay time variation as shown in Fig. 9 (Top) depends on both the signal amplitude, the threshold value, and the integrated circuit itself. Since the standard deviation is less than 3 ms, it shows that the sensor circuit meets the medical standard tolerance of ECG delineation, which is 10 ms for the onset of the P wave and 6.5 ms for the onset of Q wave [32]. Fig. 9 (Bottom) presents the measured result of the mean response time for both UTP and DTP as a function of the input slope variation and the DC voltage of the turning point. The input slope variation is measured by the ratio between the slope difference (before and after the turning point) and the turning time.

The input slope variation is measured by counting the number of the output pulses in the pulse cluster after the turning point. Since most of the information in ECG signal is below 100Hz [44], based on our prior research experience [28], we believe 1 kS/s is enough to cover the signal bandwidth. Since the sampling rate is 1 kS/s, the turning time of an abrupt turning point is considered as 1 ms. The slope variation is measured using the unit mV/ms^2. In our experiment, we use a 20 clock cycle window to count the number of pulses. Fig. 10 (Top) measures the mean output pulse density versus the input slope variation at different DC levels of the turning points. The output pulse density is proportional to the input slope variation except when the input DC level is close to the power rails. Fig. 10 (Bottom) presents the statistical distribution of the output pulse density with linearity increased input slope variation when the input DC level is in the middle between

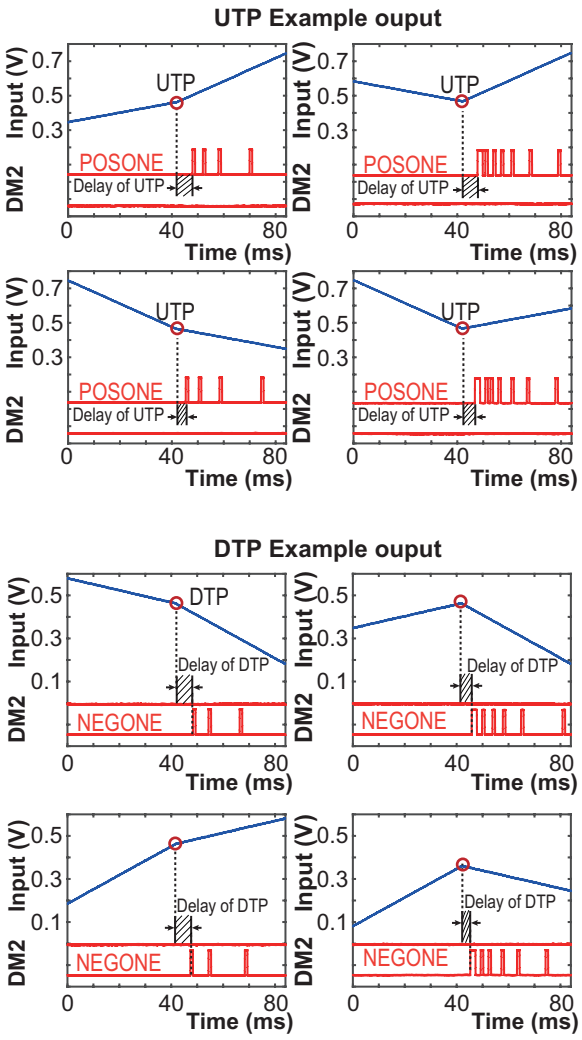

Fig. 8. Measured waveforms of the analog input turning points and the output digital bitstream with delays, (Top) Upward turning points (Bottom) Downward turning points. Modified from [14].

the power rails.

The minimum and maximum measurable input slope variation rates depend on the sampling frequency, integration gain, and the DC level of the turning point. If the slope variation is too small, the delay time may increase and become unstable. The minimum measurable slope variation means the input turning point can stably stimulate an output pulse within 20 clock cycles after the turning point. The minimum measurable slope variation is also defined as the sensitivity of the second-order Delta modulator. In our experiment, the minimum input slope variation is 3.2 mV/ms^2. On the other side, the second Delta modulator starts overloading when the maximum input slope generates consecutive pulses in the 20-clock cycle window. The measured maximum slope variation in our system is 27.2 mV/ms^2. The ratio between the maximum and minimum input slope variation of the second Delta modulator is defined as the dynamic range, which is 18.6 dB in our system.

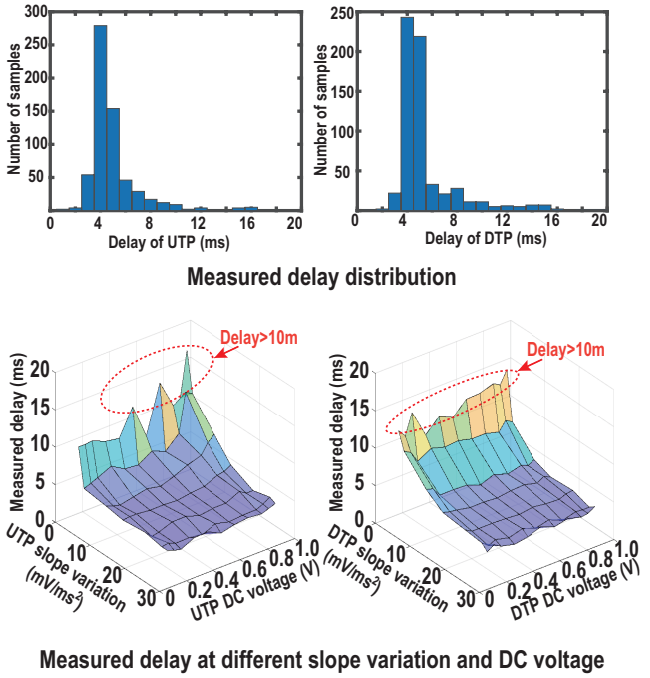

Fig. 9. (Top) Measured response time (delay) distribution of the second-order Delta modulator with different slope variations, (Bottom) mean response time with different slope variations and the DC voltages of the turning points. Modified from [14].

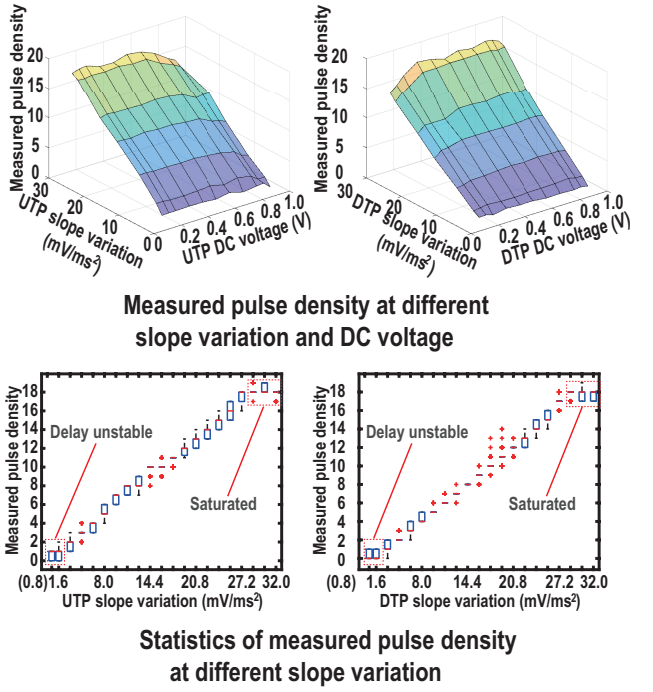

Fig. 10. (Top) Measured output pulse density of the second-order Delta modulator in a 20-bit measuring window at different slope variations and DC voltages. (Bottom) Statistics of the output pulse density versus the input slope variation. Modified from [14].

TABLE I
PERFORMANCE SUMMARY AND COMPARISON TO STATE-OF-THE-ART ECG SENSORS.

	This work	[45] JSSC19	[32] JBHI18	[28] TBCAS18	[4] JSSC16	[46] JSSC14	[23] BioCAS19	[24] ISSCC14	[25] ASSCC18
Function*	1-4	2	1-4	1-4	2	1-3	2-3	2	2
Method	Second Order Delta Modulator	Proportional Derivative Control	Second Derivative + FIR Filter	First Order Delta Modulator	Level Crossing ADC	Wavelet + Zero Crossing	SAR ADC Multi-level SVM	SAR ADC Frequency Analysis	SAR ADC Adaptive Decision
Process	180nm	65nm	MCU	130nm	130nm	180nm	180nm	65nm	180nm
Power Supply	1.0 V	0.55 V	3.7 V	$\pm$ 0.6 V	1.2 V	0.5 V	1.0 V	0.6 V	1.0 V
Sampling Rate	1 kS/s	2 kS/s	0.25 kS/s	1 kS/s	Asynch-ronous	3 kS/s	1 kS/s	0.5 kS/s	2 kS/s
Power (ADC + Detection)	151 nW	830 nW	990 nW	360 nW	$<$1 μW	457 nW	910 nW	45 nW	115 nW
Timing Error m$\pm$s	5.3$\pm$2.4 ms	N/A	22.3$\pm$14 ms	14.9$\pm$15.1 ms	N/A	N/A	N/A	N/A	N/A
Area (mm^2)	0.62$\times$0.4	1.5$\times$1	N/A	0.52$\times$0.56	0.7$\times$0.9	2$\times$2	0.6$\times$0.3	1.45$\times$2.29	0.375$\times$0.375

* Functions: (1) P wave detection; (2) R wave detection; (3) T wave detection; (4) onset/offset detection of P/T wave and QRS complex.

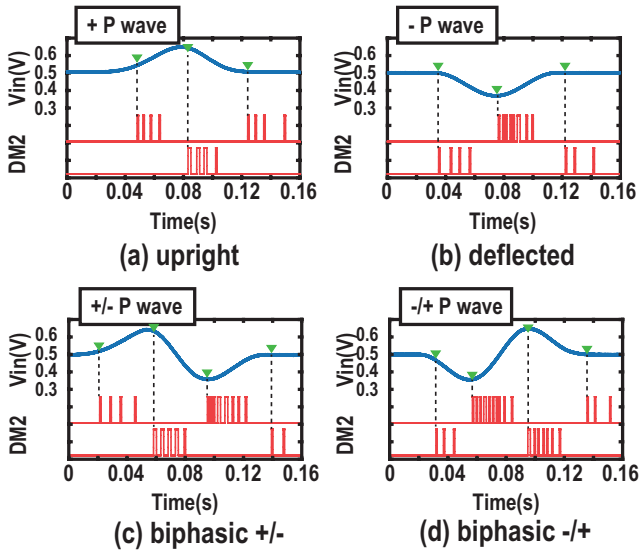

Fig. 11. The proposed prototype categorizing the morphology of the P waves by identifying the pattern of UTP and DTP (a) upright (b) negatively deflected (c) biphasic (+/-) (d) biphasic (-/+). Modified from [14].

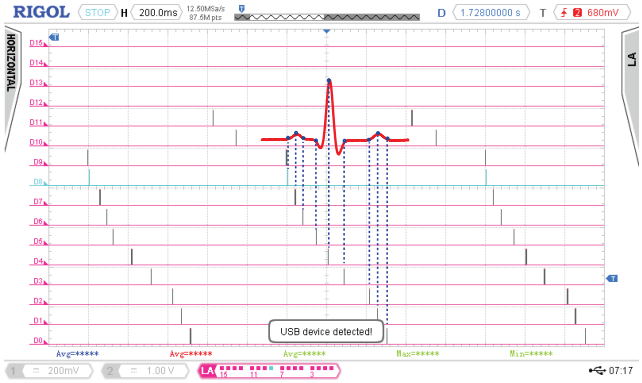

Fig. 12. Delineation testing from an oscilloscope using the second-order Delta modulator chip. The delineation algorithm is implemented on an FPGA.

B. Delineation System Testing Results

The digital signal processing of the bit-stream for delineation is performed on a Spartan6 XC6SLX9 FPGA board. The hardware system is tested using integrated circuits of the second-order Delta modulator. The input signal is an imitative normal ECG signal. The P wave morphology is classified as upright, negatively deflected, and biphasic by the order and types of the pulse clusters in the second-order Delta modulator output, as illustrated in Fig. 11. The morphology of the P wave is more important in common arrhythmia classification such as Sinus, Atrial, Atrioventricular Block (AVB), Junctional, and Premature Complex (PVC, PAC, PJC), which are required for the nurses to pass the national ECG exams. Such common arrhythmias usually do not involve the timing and morphology of T waves. The T wave is usually associated with more acute and severe conditions. To fairly compare the results with other references, this paper focuses on the classification between VEB and SVEB, which also excludes T waves. However, the T wave detection method is also important and has been covered in this paper. In the future, we are going to test advanced

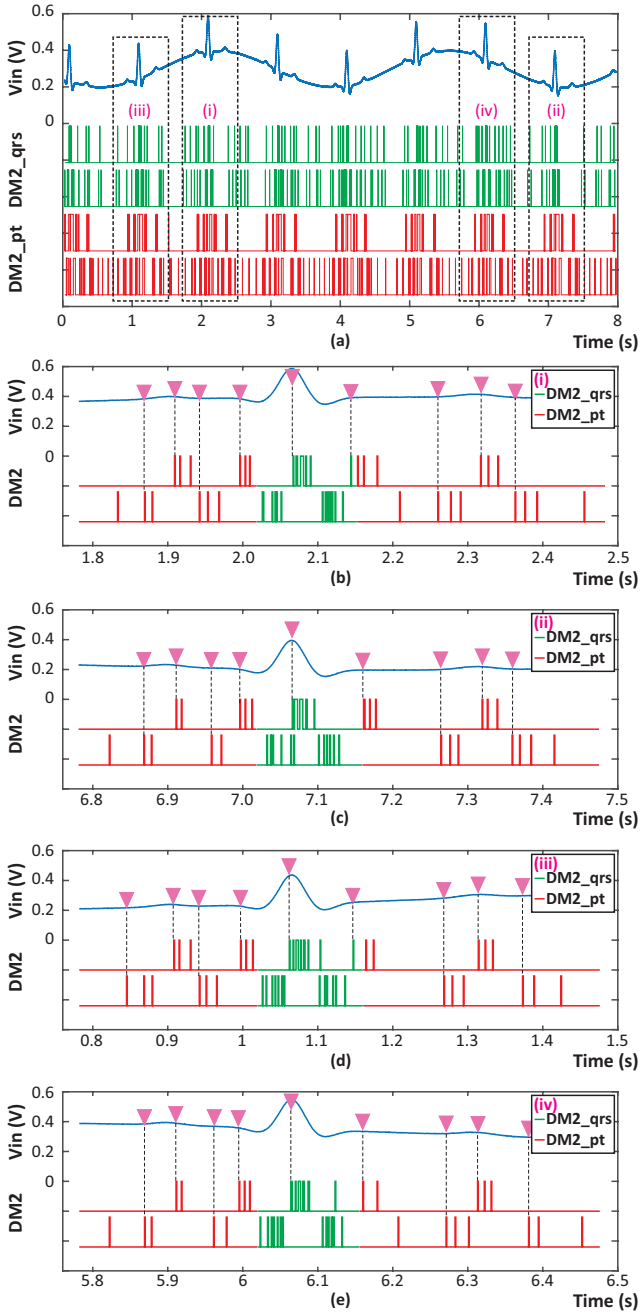

Fig. 13. Measured ECG delineation using the second-order Delta modulator chip and the FPGA. The system is robust to baseline wandering.

software and hardware systems to address more sophisticated arrhythmia classification which involves the morphology of the T waves.

Fig. 12 presents the screenshot of the digital oscilloscope that marks the fiducial points of the input ECG signal. Fig. 13 shows that the system is robust to baseline wandering even when the baseline amplitude is the same as the R peak. This is a unique feature of the proposed system thanks to the property of the second-order Delta modulator. Table I summarizes the performance of the proposed ECG sensor and compares results from recent related references.

C. Delineation and classification performance

The delineation system is also validated using all the 48 records in the MIT-BIH Arrhythmia Database for the QRS detection. Following the methods in [28], the performance of the QRS detection algorithm is evaluated by three parameters, which include the sensitivity (Se), the positive prediction (PPV), and the detection error ($Error$). In addition, for the R peak detection, m and s values are simulated, where m represents the mean errors in the time domain between the cardiologist annotations and the detection by the proposed algorithm while s stands for the average of the intra-recording standard deviations. The simulated results are illustrated in Table II.

The first 500 beats of each recording in I_g plus a basis dataset are selected to train the local classifiers while all data in T_g are selected for training the global classifier. Then the rest data of each recording in I_g are used for inference to evaluate the proposed classifier and the performance of the system. In case that a certain heartbeat class may not be included in the local training set due to the limited data volume (which make the local classifier invalid), records 209 and 215 are selected to be added into the local classifier's training dataset as the basis dataset, plus the patient dependent training set (500 samples).

The performance of the arrhythmia classification system is validated by simulation with the features extracted after delineation using the data in the MIT-BIH arrhythmia database with AAMI standard. The five parameters that are used for evaluating the performance include the F1 score ($F1$), accuracy (ACC), sensitivity (SE), specificity(SP), and positive predictive value (PPV). They are calculated using the true-positive (TP), true-negative (TN), false-positive (FP), and false-negative (FN) values. The 22-fold cross-validation is performed using the method of [34] and applied to T_g, for assessing the classifier performance and finding the optimum weights. The folds were split into training data that includes 21 folds with each fold containing one recording, and test data containing data from the remaining fold (recording). According to the AAMI standard, the heartbeats in the MIT-BIH Arrhythmia database are divided into five classes, class N for heartbeats originating in sinus node, S for SVEB, V for VEB, F for fusion beats, and Q for unknown beats. The overall performance of five classes of heartbeats is shown in Table III.

We follow the scope of the recent references that focused on the VEB and SVEB classification. VEB and SVEB are chosen since they are the most important types of arrhythmias to be classified. Thus, two binary classifications are performed, SVEBs vs non-SVEBs and VEBs vs non-VEBs. The average classification performance compared with recent references are presented in Table IV. The detailed evaluation of each patient in I_g is reported in Table V. For SVEB classification, the F1 score, sensitivity, specificity, and positive predictivity value are 0.82, 88.8%, 98.9%, and 76.1%, respectively, and for VEB classification, the numbers are 0.95, 95.1%, 99.7%, and 95.2%, respectively. The accuracy of the SVEB and VEB

TABLE II
PERFORMANCE OF THE PROPOSED QRS DETECTORS

ID	Total Peaks	FN	FP	Se (%)	PPV (%)	Error (%)	m (ms)	s (ms)
100	2273	0	0	100.00	100.00	0.00	5.26	1.30
101	1865	3	4	99.84	99.79	0.38	1.59	2.48
102	2187	0	0	100.00	100.00	0.00	-1.19	11.70
103	2084	6	0	99.71	100.00	0.29	5.92	1.23
104	2229	2	0	99.91	100.00	0.09	-6.09	16.02
105	2572	37	8	98.56	99.69	1.75	2.55	2.67
106	2027	60	2	97.04	99.90	3.06	2.16	5.97
107	2137	8	1	99.63	99.95	0.42	-3.77	2.04
108	1763	118	18	93.31	98.82	7.71	-24.33	23.72
109	2532	24	0	99.04	100.00	0.95	1.12	5.45
111	2124	4	6	99.81	99.72	0.47	-36.52	11.54
112	2539	0	1	100.00	99.96	0.04	4.79	2.24
113	1795	1	0	99.94	100.00	0.06	4.50	1.09
114	1879	4	2	99.79	99.89	0.32	10.19	14.06
115	1953	0	0	100.00	100.00	0.00	6.80	1.14
116	2412	29	3	98.80	99.87	1.33	6.01	3.08
117	1535	0	1	100.00	99.93	0.07	-17.41	7.18
118	2278	3	1	99.87	99.96	0.18	4.37	7.07
119	1987	1	1	99.95	99.95	0.10	3.95	5.85
121	1863	4	1	99.79	99.95	0.27	-1.39	3.46
122	2476	1	1	99.96	99.96	0.08	0.88	1.68
123	1518	3	0	99.80	100.00	0.20	6.55	1.16
124	1619	11	0	99.32	100.00	0.68	0.72	4.27
200	2601	15	4	99.42	99.85	0.73	-3.03	17.92
201	1963	76	0	96.13	100.00	3.87	5.68	1.92
202	2136	12	0	99.44	100.00	0.56	5.06	1.44
203	2980	139	37	95.34	98.71	5.91	-4.32	15.93
205	2656	4	0	99.85	100.00	0.15	2.92	6.20
207	2332	268	75	88.51	96.49	14.71	-28.38	34.30
208	2955	46	18	98.44	99.39	2.17	9.15	13.51
209	3005	8	6	99.73	99.80	0.47	5.69	1.41
210	2650	30	17	98.87	99.36	1.77	0.48	7.64
212	2748	1	3	99.96	99.89	0.15	5.37	1.81
213	3251	2	1	99.94	99.97	0.09	1.59	8.34
214	2262	9	2	99.60	99.91	0.49	4.69	4.49
215	3363	8	1	99.76	99.97	0.27	5.10	3.55
217	2208	9	2	99.59	99.91	0.50	-14.63	11.70
219	2154	0	0	100.00	100.00	0.00	2.55	3.57
220	2048	0	0	100.00	100.00	0.00	6.83	2.38
221	2427	7	2	99.71	99.92	0.37	4.09	3.82
222	2483	6	7	99.76	99.72	0.52	3.39	4.16
223	2605	1	1	99.96	99.96	0.08	3.58	8.71
228	2053	40	29	98.05	98.58	3.36	1.35	7.88
230	2256	0	2	100.00	99.91	0.09	7.76	1.64
231	1571	0	0	100.00	100.00	0.00	2.96	1.16
232	1780	3	1	99.83	99.94	0.22	7.35	1.91
233	3079	10	1	99.68	99.97	0.36	-3.84	15.56
234	2753	3	0	99.89	100.00	0.11	3.44	1.10
Total	109966	1016	259	99.08	99.76	1.16	0.57	12.92

TABLE III
OVERALL FIVE CLASSES OF HEARTBEATS CLASSIFICATION RESULTS

Actual classes \ Predicted classes	n	s	v	f	q
N	32969	343	124	862	6
S	137	1240	36	14	1
V	106	10	2405	8	0
F	231	23	18	11	9
Q	3	0	2	0	0

classification achieved 98.5% and 99.4%, respectively. The result of this work achieved the highest sensitivity in both SVEB and VEB classification among the related works. The global classifiers trained with and without record 209 and 215

TABLE IV
AVERAGE CLASSIFICATION RESULTS COMPARED TO THE STATE OF ART

Methods	SVEB					VEB				
	F1	ACC	SE	SP	PPV	F1	ACC	SE	SP	PPV
Hu et.al [47]	0.80	95.5	82.6	97.1	77.7	-	-	-	-	-
Ince et.al [12]	0.58	97.4	63.5	99.0	53.7	0.86	98.3	84.6	98.7	87.4
Chazal et.al [38]	0.61	95.9	87.7	96.2	47.0	0.95	99.4	94.3	99.7	96.2
Alexander et.al [11]	0.68	-	86.2	97.5	56.7	0.94	-	92.4	99.6	94.8
Li et.al [9]	0.89	99.4	85.5	99.4	92.3	0.90	98.9	88.0	98.9	92.6
Kiranyaz et.al [16]	0.62	97.6	60.3	99.2	63.5	0.92	99.0	93.9	98.9	90.6
Tang et.al [34]	0.83	98.8	79.3	99.6	88.2	0.92	99.0	92.8	99.4	91.6
Proposed DM2-22	**0.82**	**98.5**	**88.8**	**98.9**	**76.1**	**0.95**	**99.4**	**95.1**	**99.7**	**95.2**
Proposed DM2-22 *	**0.82**	**98.5**	**88.8**	**98.9**	**75.9**	**0.95**	**99.4**	**95.1**	**99.6**	**94.9**

* Overall performance of the proposed method with global classifier trained without 209 and 215.

(training basis for local classifier) show a slightly difference of the overall classification performance as shown in Table IV and the influence can be ignored.

IV. DISCUSSIONS

This paper presented a novel ternary second-order Delta modulator for monitoring electrocardiogram signals, including delineation and arrhythmia classification. The main contribution is proposing the new concept and methods of slope variation measurement of the analog signal from the bitstream generated from the second-order Delta modulator. Then the feature of slope variation is obtained directly after the analog-to-digital conversion. Based on the proposed circuits, we also proposed new algorithms to calculate the slope variation, which is characterized from the fabricated integrated circuits. New concepts for slope variation measurement, including sensitivity and dynamic range, are proposed and measured. Another contribution of the paper is the ECG delineation and classification algorithms based on the slope variation measurement. Novel feature sets are proposed for delineation and the patient-specific classification methods are applied on the bitstream data from the second-order Delta modulator. The algorithm is validated using the MIT-BIH database. The experiment results show that the performance of the system is better than a first-order Delta modulator based ECG monitoring system, as validated by the classification sensitivity. The proposed system along with the algorithm is promising for future wearable arrhythmia monitoring systems.

In future work, the second-order Delta modulator circuit could be further optimized for power reduction. For example, currently, the threshold is determined by an optimizing process through parameter analysis. The next generation of the system would include the front-end amplifier that has a variable gain with feedback gain control to form an automatic gain control (AGC) block to make sure that the measured ECG signals from the analog-front-end have a relatively stable amplitude. The AGC is based on our QRS detection algorithm and the slope variation extracted from the output bitstream of the proposed second order ternary Delta modulator. If the QRS detection algorithm cannot detect the target for a certain time, it assumes the signal amplitude is not large enough, so the AGC can adjust the variable gain amplifier (VGA) to amplify the input ECG signal, and vice versa. The front-end amplifier

TABLE V
CLASSIFICATION RESULTS FOR EACH OF THE TEST PATIENTS

	Number of Beats			Number of Beats Detected				SVEB					VEB				
REQ	N+F+Q	S	V	N+F+Q	S	V	FP	F1	ACC	SE	PPV	SP	F1	ACC	SE	PPV	SP
100	1744	28	1	1742	28	1	1	0.59	98.59	64.29	54.55	99.14	1	100.00	100.00	100.00	100.00
103	1582	2	0	1574	2	0	0	0	99.87	0.00	-	100.00	-	100.00	-	-	100.00
105	2046	0	26	2015	0	26	144	-	100.00	-	-	100.00	0.75	99.17	96.15	60.98	99.21
111	1623	0	1	1623	0	1	7	-	100.00	-	-	100.00	0	99.94	0.00	-	100.00
113	1293	2	0	1290	2	0	0	0.44	99.61	100.00	28.57	99.61	-	100.00	-	-	100.00
117	1034	1	0	1033	1	0	1	1	100.00	100.00	100.00	100.00	-	100.00	-	-	100.00
121	1361	1	1	1356	1	1	3	0	99.93	0.00	-	100.00	1	100.00	100.00	100.00	100.00
123	1016	0	2	1013	0	0	0	-	100.00	-	-	100.00	-	100.00	-	-	100.00
200	1392	28	681	1391	28	669	36	0.17	97.27	21.43	14.63	98.30	0.96	97.37	91.78	100.00	100.00
202	1570	54	12	1568	47	7	0	0.64	97.72	70.21	58.93	98.54	0.35	99.32	42.86	30.00	99.57
210	1968	20	162	1958	19	158	4	0.49	99.02	52.63	45.45	99.43	0.92	98.83	90.51	93.46	99.49
212	2248	0	0	2248	0	0	4	-	100.00	-	-	100.00	-	100.00	-	-	100.00
213	2525	27	199	2523	27	198	0	0.63	99.34	55.56	71.43	99.78	0.84	97.31	95.96	74.22	97.41
214	1565	0	197	1557	0	196	0	-	100.00	-	-	100.00	0.97	99.32	94.39	99.46	99.94
219	1604	3	47	1602	3	47	0	0	99.82	0.00	-	100.00	0.97	99.82	95.75	97.83	99.94
221	1626	0	301	1623	0	297	0	-	100.00	-	-	100.00	0.99	99.69	97.98	100.00	100.00
222	1774	209	0	1774	208	0	8	0.47	82.59	72.12	34.32	83.82	0	99.24	-	0.00	99.24
228	1300	3	250	1298	3	239	50	0	99.81	0.00	-	100.00	0.98	99.48	96.65	100.00	100.00
231	1071	0	0	1069	0	0	0	-	100.00	-	-	100.00	-	100.00	-	-	100.00
232	271	1009	0	271	1005	0	10	1	99.69	99.90	99.70	98.89	-	100.00	-	-	100.00
233	1879	4	696	1875	4	689	0	0	99.84	0.00	-	100.00	0.99	99.34	98.26	99.27	99.73
234	2200	50	3	2198	50	0	0	0.63	98.49	58.00	69.05	99.41	-	100.00	-	-	100.00

also performs noise filtering. The oversampling rate may be reduced to save system power and computing overhead. Since the proposed system performs a full delineation of the ECG signal, it could be applied to the detection of more elaborate types of arrhythmia, such as distinguishing Atrial Premature Beat (APB), PVC, Left Bundle Branch Block (LBBB), etc. The delineation accuracy may be improved by combining other analog-to-feature-conversion circuits and systems such as the first-order Delta modulator or Sigma-Delta modulator. Clinical testing using an ECG signal directly from a physical ECG sensor would be helpful to further evaluate the performance of the proposed system. In future work, the current 22 features could also be optimized or reduced to save computing overhead.

This work focuses on ECG signal processing instead of ECG signal acquisition. So, we assume that the front-end circuit would have enough gain to ensure the amplitude of the input signal. In fact, in our experiment we used a signal generator to provide the input signal. In the real application, the system should have a front-end circuit to perform signal amplification and perform noise filtering, which will be studied in our future work. The ultimate goal is to perform human subject testing to evaluate the performance of the proposed system as wearable sensors that can perform on-chip arrhythmia classification. Although the proposed system can handle baseline wandering, the system is not designed for ambulatory monitoring where motion artifacts can be large. Besides, although hardware-efficient implementation is emphasized, the patient-specific linear kernel may not provide high classification performance compared to the RBF kernel.

V. CONCLUSION

An ECG monitoring and arrhythmia classification system has been presented. The system applies a parallel ternary second-order Delta modulator to convert the ECG signal to two channels of ternary bit-streams for QRS complex monitoring and P/T wave monitoring. The bitstream is a pulse density modulation of the slope variation of the input analog signal. The ternary second-order Delta modulator chip is fabricated and tested for recording slope variation of the input ECG signal without measuring the instantaneous amplitude. The sensitivity of the slope variation measurement is 3.2 mV/ms^2 and the dynamic range is 18.6 dB. The chip consumes 151 nW when sampling at 1 kS/s. The measured slope variations are applied to ECG delineation, which detects the fiducial points in ECG waves. We proposed a delineation algorithm based on the second-order Delta modulated bitstream, which detects the fiducial points of the ECG signals and has been tested in an FPGA prototype along with the second-order Delta modulator chip. A feature set including 22 features has been designed for arrhythmia classification. A rotation linear kernel SVM is applied for arrhythmia classification. The classification algorithm is verified through the MIT-BIH Arrhythmia Database. Two binary classifications are performed and evaluated according to the AAMI standard including SVEB, VEB, and the heartbeats originating in sinus node. The sensitivity of the SVEB and VEB classification achieved 88.8% and 95.1%, respectively. The proposed system is promising for future wearable ECG monitoring systems with interpretable machine learning.

REFERENCES

[1] "New initiative launched to tackle cardiovascular disease, the world's number one killer." [Online]. Available: http://www.who.int/cardiovascular_diseases/en/

[2] E. J. Benjamin, S. S. Virani, C. W. Callaway, A. M. Chamberlain, A. R. Chang, S. Cheng, S. E. Chiuve, M. Cushman, F. N. Delling, R. Deo *et al.*, "Heart disease and stroke statistics 2018 update: a report from the American Heart Association," *Circulation*, vol. 137, no. 12, pp. e67–e492, 2018.

[3] H. C. McGill Jr, C. A. McMahan, and S. S. Gidding, "Preventing heart disease in the 21st century: implications of the Pathobiological

Determinants of Atherosclerosis in Youth (PDAY) study," *Circulation*, vol. 117, no. 9, pp. 1216–1227, 2008.

[4] X. Zhang, Z. Zhang, Y. Li, C. Liu, Y. X. Guo, and Y. Lian, "A 2.89-μ W Dry-Electrode Enabled Clockless Wireless ECG SoC for Wearable Applications," *IEEE Journal of Solid-State Circuits*, vol. 51, no. 10, pp. 2287–2298, 2016.

[5] D. Da He and C. G. Sodini, "A 58 nW ECG ASIC with motion-tolerant heartbeat timing extraction for wearable cardiovascular monitoring," *IEEE Transactions on Biomedical Circuits and Systems*, vol. 9, no. 3, pp. 370–376, 2015.

[6] C.-I. Ieong, P.-I. Mak, C.-P. Lam, C. Dong, M.-I. Vai, P.-U. Mak, S.-H. Pun, F. Wan, and R. P. Martins, "A 0.83-QRS detection processor using quadratic spline wavelet transform for wireless ECG acquisition in 0.35-CMOS," *IEEE Trans. Biomed. Circuits Syst*, vol. 6, no. 6, pp. 586–595, 2012.

[7] Y. Chuo, M. Marzencki, B. Hung, C. Jaggernauth, K. Tavakolian, P. Lin, and B. Kaminska, "Mechanically flexible wireless multisensor platform for human physical activity and vitals monitoring," *IEEE Transactions on Biomedical Circuits and Systems*, vol. 4, no. 5, pp. 281–294, 2010.

[8] S. Raj and K. C. Ray, "ECG signal analysis using DCT-based DOST and PSO optimized SVM," *IEEE Transactions on Instrumentation and Measurement*, vol. 66, no. 3, pp. 470–478, 2017.

[9] P. Li, Y. Wang, J. He, L. Wang, Y. Tian, T.-s. Zhou, T. Li, and J.-s. Li, "High-performance personalized heartbeat classification model for long-term ECG signal," *IEEE Transactions on Biomedical Engineering*, vol. 64, no. 1, pp. 78–86, 2017.

[10] C. Ye, B. V. Kumar, and M. T. Coimbra, "Heartbeat classification using morphological and dynamic features of ECG signals," *IEEE Transactions on Biomedical Engineering*, vol. 59, no. 10, pp. 2930–2941, 2012.

[11] A. S. Alvarado, C. Lakshminarayan, and J. C. Principe, "Time-based compression and classification of heartbeats," *IEEE Transactions on Biomedical Engineering*, vol. 59, no. 6, p. 1641, 2012.

[12] T. Ince, S. Kiranyaz, and M. Gabbouj, "A generic and robust system for automated patient-specific classification of ECG signals," *IEEE Transactions on Biomedical Engineering*, vol. 56, no. 5, pp. 1415–1426, 2009.

[13] A. Y. Hannun, P. R. P. Rajpurkar, M. Haghpanahi, G. H. Tison, C. Bourn, M. P. Turakhia, and A. Y. Ng, "Cardiologist-level arrhythmia detection and classification in ambulatory electrocardiograms using a deep neural network," *Nature medicine*, vol. 25, no. 1, pp. 65–69, 2019.

[14] X. Tang and W. Tang, "A 151nW Second-Order Ternary Delta Modulator for ECG Slope Variation Measurement with Baseline Wandering Resilience," in *2020 IEEE Custom Integrated Circuits Conference (CICC)*, 2020, pp. 1–4.

[15] P. De Chazal, M. O'Dwyer, and R. B. Reilly, "Automatic classification of heartbeats using ECG morphology and heartbeat interval features," *IEEE Transactions on Biomedical Engineering*, vol. 51, no. 7, pp. 1196–1206, 2004.

[16] S. Kiranyaz, T. Ince, and M. Gabbouj, "Real-time patient-specific ECG classification by 1-D convolutional neural networks," *IEEE Transactions on Biomedical Engineering*, vol. 63, no. 3, pp. 664–675, 2016.

[17] J. Yoo, L. Yan, D. El-Damak, M. A. B. Altaf, A. H. Shoeb, and A. P. Chandrakasan, "An 8-Channel Scalable EEG Acquisition SoC With Patient-Specific Seizure Classification and Recording Processor," *IEEE Journal of Solid-State Circuits*, vol. 48, no. 1, pp. 214–228, Jan 2013.

[18] V. Sze, Y.-H. Chen, J. Emer, A. Suleiman, and Z. Zhang, "Hardware for machine learning: Challenges and opportunities," in *Custom Integrated Circuits Conference (CICC), 2018 IEEE*, pp. 1–8.

[19] S. Kadambe, R. Murray, and G. F. Boudreaux-Bartels, "Wavelet transform-based QRS complex detector," *IEEE Transactions on biomedical Engineering*, vol. 46, no. 7, pp. 838–848, 1999.

[20] C. I. Ieong, P. I. Mak, C. P. Lam, C. Dong, M. I. Vai, P. U. Mak, S. H. Pun, F. Wan, and R. P. Martins, "A 0.83-$murmW$ QRS Detection Processor Using Quadratic Spline Wavelet Transform for Wireless ECG Acquisition in 0.35- $murmm$ CMOS," *IEEE Transactions on Biomedical Circuits and Systems*, vol. 6, no. 6, pp. 586–595, Dec 2012.

[21] J. P. Martinez, R. Almeida, S. Olmos, A. P. Rocha, and P. Laguna, "A wavelet-based ECG delineator: evaluation on standard databases," *IEEE Transactions on Biomedical Engineering*, vol. 51, no. 4, pp. 570–581, April 2004.

[22] F. Rincón, J. Recas, N. Khaled, and D. Atienza, "Development and Evaluation of Multilead Wavelet-Based ECG Delineation Algorithms for Embedded Wireless Sensor Nodes," *IEEE Transactions on Information Technology in Biomedicine*, vol. 15, no. 6, pp. 854–863, Nov 2011.

[23] M. A. Sohail, Z. Taufique, S. M. Abubakar, W. Saadeh, and M. A. Bin Altaf, "An ECG Processor for the Detection of Eight Cardiac Arrhythmias with Minimum False Alarms," in *2019 IEEE Biomedical Circuits and Systems Conference (BioCAS)*, 2019, pp. 1–4.

[24] D. Jeon, Y. P. Chen, Y. Lee, Y. Kim, Z. Foo, G. Kruger, H. Oral, O. Berenfeld, Z. Zhang, D. Blaauw, and D. Sylvester, "An implantable 64nW ECG-monitoring mixed-signal SoC for arrhythmia diagnosis," in *2014 IEEE International Solid-State Circuits Conference Digest of Technical Papers (ISSCC)*, 2014, pp. 416–417.

[25] S. M. Abubakar, M. Rizwan Khan, W. Saadeh, and M. A. Bin Altaf, "A Wearable Auto-Patient Adaptive ECG Processor for Shockable Cardiac Arrhythmia," in *2018 IEEE Asian Solid-State Circuits Conference (A-SSCC)*, 2018, pp. 267–268.

[26] X. Tang, Q. Hu, and W. Tang, "Analog to Digital Feature Converter based on Oversampling Modulators for ECG Delineation," in *2019 IEEE 62nd International Midwest Symposium on Circuits and Systems (MWSCAS)*, 2019, pp. 121–124.

[27] Y. Liu, P. M. Furth, and W. Tang, "Hardware-efficient delta sigma-based digital signal processing circuits for the internet-of-things," *Journal of Low Power Electronics and Applications*, vol. 5, no. 4, p. 234, 2015. [Online]. Available: http://www.mdpi.com/2079-9268/5/4/234

[28] X. Tang, Q. Hu, and W. Tang, "A Real-Time QRS Detection System With PR/RT Interval and ST Segment Measurements for Wearable ECG Sensors Using Parallel Delta Modulators," *IEEE Transactions on Biomedical Circuits and Systems*, vol. 12, no. 4, pp. 751–761, 2018.

[29] D. Zrilic, G. Petrovic, and W. Tang, "Novel solutions of a deltasigma-based rectifying encoder," *IEEE Transactions on Circuits and Systems II: Express Briefs*, vol. 64, no. 10, pp. 1242–1246, 2017.

[30] X. Tang, Q. Hu, and W. Tang, "Delta Sigma Encoder for Low-Power Wireless Bio-Sensors Using Ultrawideband Impulse Radio," *IEEE Transactions on Circuits and Systems II: Express Briefs*, vol. 64, no. 7, pp. 747–751, 2017.

[31] R. Rieger and S.-H. Nian, "Integrated control circuit for adaptive sampling," *Analog Integrated Circuits and Signal Processing*, vol. 72, no. 1, pp. 227–235, 2012.

[32] J. M. Bote, J. Recas, F. Rincón, D. Atienza, and R. Hermida, "A Modular Low-complexity ECG Delineation Algorithm for Real-time Embedded Systems," *IEEE Journal of Biomedical and Health Informatics*, vol. 22, no. 2, pp. 429–441, 2017.

[33] Association for the Advancement of Medical Instrumentation and others, "Testing and reporting performance results of cardiac rhythm and ST segment measurement algorithms," *ANSI/AAMI EC38*, vol. 1998, 1998.

[34] X. Tang, Z. Ma, Q. Hu, and W. Tang, "A real-time arrhythmia heartbeats classification algorithm using parallel delta modulations and rotated linear-kernel support vector machines," *IEEE Transactions on Biomedical Engineering*, pp. 1–1, 2019.

[35] R. S. Assaad and J. Silva-Martinez, "The Recycling Folded Cascode: A General Enhancement of the Folded Cascode Amplifier," *IEEE Journal of Solid-State Circuits*, vol. 44, no. 9, pp. 2535–2542, 2009.

[36] R. Jeongjin, B. Sanho, C. Youngkil, R. Hyungdong, K. Yi-Gyeong, and K. Jong-Kee, "A 0.9-V 60-mW 1-bit Fourth-order Delta–sigma Modulator with 83-dB Dynamic Range," *IEEE Journal of Solid-State Circuits*, vol. 43, pp. 361–370, 2008.

[37] K. H. Lee and N. Verma, "A low-power processor with configurable embedded machine-learning accelerators for high-order and adaptive analysis of medical-sensor signals," *IEEE Journal of Solid-State Circuits*, vol. 48, no. 7, pp. 1625–1637, 2013.

[38] P. de Chazal and R. B. Reilly, "A patient-adapting heartbeat classifier using ECG morphology and heartbeat interval features," *IEEE Transactions on Biomedical Engineering*, vol. 53, no. 12, pp. 2535–2543, 2006.

[39] J. Wang, R. Li, R. Li, B. Fu, C. Xiao, and D. Z. Chen, "Towards interpretable arrhythmia classification with human-machine collaborative knowledge representation," *IEEE Transactions on Biomedical Engineering*, pp. 1–1, 2020.

[40] F. Alonso-Atienza, E. Morgado, L. Fernandez-Martinez, A. García-Alberola, and J. L. Rojo-Alvarez, "Detection of life-threatening arrhythmias using feature selection and support vector machines," *IEEE Trans. Biomed. Eng*, vol. 61, no. 3, pp. 832–840, 2014.

[41] Q. Li, C. Rajagopalan, and G. D. Clifford, "Ventricular fibrillation and tachycardia classification using a machine learning approach," *IEEE Transactions on Biomedical Engineering*, vol. 61, no. 6, pp. 1607–1613, 2014.

[42] S. Osowski, L. T. Hoai, and T. Markiewicz, "Support vector machine-based expert system for reliable heartbeat recognition," *IEEE Transactions on Biomedical Engineering*, vol. 51, no. 4, pp. 582–589, 2004.

[43] M. Llamedo and J. P. Martínez, "Heartbeat classification using feature selection driven by database generalization criteria," *IEEE Transactions on Biomedical Engineering*, vol. 58, no. 3, pp. 616–625, 2011.
[44] A. Ziarani and A. Konrad, "A nonlinear adaptive method of elimination of power line interference in ECG signals," *IEEE Transactions on Biomedical Engineering*, vol. 49, no. 6, pp. 540–547, 2002.
[45] S. Yin, M. Kim, D. Kadetotad, Y. Liu, C. Bae, S. J. Kim, Y. Cao, and J.-s. Seo, "A 1.06-μW Smart ECG Processor in 65-nm CMOS for Real-Time Biometric Authentication and Personal Cardiac Monitoring," *IEEE Journal of Solid-State Circuits*, 2019.
[46] X. Liu, J. Zhou, Y. Yang, B. Wang, J. Lan, C. Wang, J. Luo, W. L. Goh, T. T.-H. Kim, and M. Je, "A 457 nW Near-threshold Cognitive Multi-functional ECG Processor for Long-term Cardiac Monitoring," *IEEE Journal of Solid-State Circuits*, vol. 49, no. 11, pp. 2422–2434, 2014.
[47] Y. H. Hu, S. Palreddy, and W. J. Tompkins, "A patient-adaptable ECG beat classifier using a mixture of experts approach," *IEEE Transactions on Biomedical Engineering*, vol. 44, no. 9, pp. 891–900, 1997.

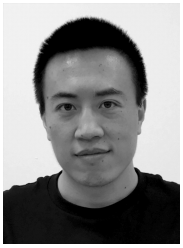

Xiaochen Tang (Member, IEEE) received the B.E. degree in electronics science and technology and the M.E. degree in microelectronics and solid-state electronics from the Harbin Institute of Technology, Harbin, China, in 2010 and 2012, respectively, and the Ph.D. degree in electrical engineering from New Mexico State University, Las Cruces, USA, in 2020. He is currently a Postdoctoral Researcher with Texas AM University, College Station, TX, USA. His research interests include low-power biomedical integrated circuits and wearable biomedical devices.

Wei Tang (Member, IEEE) received the B.Sc. degree in microelectronics from Peking University, Beijing, China, in 2006, and the Ph.D. degree in electrical engineering from Yale University, New Haven, CT, USA, in 2012. He joined the Klipsch School of Electrical and Computer Engineering, New Mexico State University, Las Cruces, NM, USA, as an Assistant Professor in 2012, where he was promoted to an Associate Professor in 2018. He is currently an Associate Professor with the Klipsch School of Electrical and Computer Engineering, New Mexico State University. His research interests include low-power analog/mixed-signal/digital/RF integrated circuits design and implementation, hardware-friendly digital signal processing and image processing algorithms, and biomedical sensors and wearable devices, circuits and systems. He was a recipient of the National Science Foundation Faculty Early Career Award in 2017 and currently holds the Paul W. and Valerie Klipsch Distinguished Professorship of New Mexico State University.